Available online at www.sciencedirect.com

SciVerse ScienceDirect

Physics Procedia 41 (2013) 448 – 459

Physics Procedia

Lasers in Manufacturing Conference 2013

Nd:YAG laser welding of sheet metal assembly: Transformation induced volume strain affect on elastoplastic model

C. Seang[a*], A.K. David[b], E. Ragneau[b]

[a]*20, avenue des Buttes de Coesmes 35708, phone: 032-23-2323 8516; e-mail: seang@insa-rennes.fr.*
[b]*20, avenue des Buttes de Coesmes 35708, phone: 032-23-2323 8614; e-mail: akouadri@insa-rennes.fr*

Abstract

This study presents the effect of transformation induced volume strain on the thermo-elastoplastic model in the simulation of Nd: YAG laser welding process applied for thin sheet metal dual phases steel DP600. The metallurgical phase transformations during heating and during cooling are used as the thermal expansion dependent parameters. The effect of transformation induced volumetric strain was identified where the comparisons of the elastoplastic model with and without metallurgical effect are based on the global distribution of residual stresses such as the longitudinal residual stresses and the transverse residual stresses.

Keywords: Nd YAG laser welding, Abaqus, Phase transformation, Residual stresses;

1. Introduction

The phase transformation affects the welding process in a number of ways. Under the transformation induced volume strain effect, it influences the welding distortion and stresses due to their accompanied volume expansion [20] which is theoretically 1.3% of volume expansion for the austenite - ferrite transformation and 4% for austenite - martensite transformation [21]. If 100% ferrite is transformed to 100% martensite, due to heat treatment, the results in a volume different of 2.7%. In order to predict the welding stresses and distortions as adequate as possible, it appears to be indispensable to incorporate phase

* Corresponding author. Tel.: +33621049303
E-mail address: seangpk@gmail.com

doi:10.1016/j.phpro.2013.03.101

transformations in the model due to the strong spatial dependency of the phase transformations under effect of different cooling rates [20]. Studies performed by Taljat et al [2] indicated that this volumetric expansion on cooling phase lowers the residual stresses in the fusion zone of the weld joint. Beside the physical properties of sheet metal, the welding process plays an important factor in the formation of welding pool and its evolution during cooling phase. It affects on the heating rate, the cooling rate, the metallurgical and the mechanical property of the welded joint as mention in the previous research works. The residual stresses along the transverse line were observed by Kong [13], the numerical and X-ray diffraction analysis had been used to study the influence of different welding processes of lap joint, laser, GTAW, hybrid laser-GTAW. He found out that the maximum normal stress components are located at the HAZ and its peak value increase with the decrease in welding speed. He also notice that, from X-ray diffraction technique increasing the welding speed (1.2 m/min to 2.4m/min), the longitudinal stress at the center of the weld bead (FZ) changes from compressive state to the tensile one.

So the implement of metallurgical effect in mechanical model is important in numerical analysis of welding residual stresses and residual distortion. The elastoplastic model includes the transformation induced volumetric strain is used to compare with the classical elastoplastic model applied to the analysis of Nd: YAG laser welding of sheet metal joining process.

2. Numerical Model

The thermo-mechano-metallurgical model constitutes of three models separately, the thermal model, the metallurgical model and the mechanical model. The thermal model constitutes of heat transfer equation and heat source model. The metallurgical model used in this simulation is based on Waeckel model [7, 27, 28], Elastoplastic model is used for mechanical model.

2.1. Thermal Model

The heat transfer from the volumetric heat source to the metal during the welding phase is expressed by equation 1. The heat lose during cooling process are expressed in equation, 2 and 3. Its symbols are shown in Table 1.

$$\rho \frac{dH}{dt} - div(\lambda gradT) - Q = 0 \tag{1}$$

Two mathematical formulations applied during the cooling phase are:

- The convection limits condition on the surrounding is given by:

$$\lambda(T) gradT(x_i, t)_{surface} + H(T(x_i, t) - T_0) = 0 \tag{2}$$

- The radiation limits condition on the weld pool surface is given by:

$$\lambda(T) gradT(x_i, t)_{surface} + \varepsilon\sigma(T(x_i, t)^4 - T_\infty{}^4) = 0 \tag{3}$$

An initial condition is defined by the temperature of metal, T equal to the surrounding temperature 20˚C.

The conical heat source with Gaussian distribution [25] represented by equation 4 and 5. The parameter and symbol using in the conical heat source are presented in Tab.2 along with the figure of conical heat source.

$$Q(r,z) = \frac{6\eta P e^3}{\pi(e^3-1)} \cdot \frac{e^{-[\frac{2r^2}{r_c^2}]}}{(z_e - z_e)(r_e^2 + r_e r_i + r_i^2)} \quad (4)$$

With

$$r_c = r_i + \frac{(r_e - r_i)(z - z_i)}{z_e - z_i} \quad (5)$$

Table 1. Units for Thermal Properties

Symbol	*Quantity*	*SI* [a]
ρ	Density	kg/m^3
H	Enthalpy	J/(kg.°C)
λ	Thermal conductivity	W/(m.°C)
Q	Internal heat	W/m^3
ϵ	emissivity	0.25
σ	Stefan Boltzmann	5.670410^{-8}W/(m.K^4)
-	absolute zero	-273.15°C
t	time	s
x_i	spatial coordinate	m

[a] m = meter, J = joule, kg = kilogram, W = Watt, °C = Degree Celsius, K = Kelvin, s = second.

Table 2. Dimension of thermal model heat source

Symbol	*Quantity*	*Value*
r_e	radius superior of cone	0.8 m^{-6}
r_i	radius inferior of cone	0.35 m^{-6}
r_c	distribution parameter	m^{-6}
z_e	position in Z axis of r_e	2.6 m^{-6}
z_i	position in Z axis of r_i	0 m^{-6}
P	laser power	4000 W
η	efficiency	42%
V	welding speed	0.0567m/s

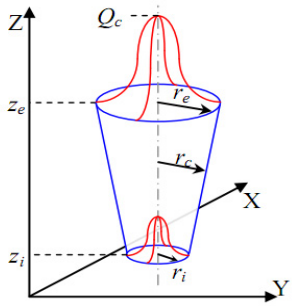

The welding speed, energy input and heat source distributions have important effects on the shape and boundaries of FZ and HAZ. It also affects the peak temperature in FZ, which consequently affect the transient temperature distributions in the welded metal [8]. The real dimension of weld pool cross section is used in this analysis. Its values are shown in Tab.2.

2.2. Metallurgical Model

The Waeckel model [7, 27, 28] allows describing the anisothermes metallurgical transformation provided by a differential equation. This model derived from model Leblond [14], base on the CCT diagram data, which is particularly suitable to describe the industrial applications such as welding. It is able to simulate all thermo-metallurgical histories and has been inserted in the thermo-mechanics finite element code, Code Aster. It is easier to identify its parameters than the model Leblond.

During heating the only transformation able to occur is the transformation into austenite which not strongly depends to the heating rate. Then the function used to describe this kind of transformation is the same as those proposed by Leblond and for which:

$$\dot{Z}_{\gamma} = \frac{Z_{eq} - z_{\gamma}}{\tau(T)} \tag{6}$$

Where z_γ denotes the austenite proportion, Z_{eq} is the change in the rate of austenite transformed during quasi-static evolution, τ represents the growth parameter (second), Z_{eq} and τ are two functions depending on temperatures.

$$Z_{eq}(T) = \begin{cases} 0 & \text{if } T \le Ac1 \\ \frac{T-Ac1}{Ac3-Ac1} & \text{if } Ac1 \le T \le Ac3 \\ 1 & \text{if } T \ge Ac3 \end{cases} \tag{7}$$

$$\tau(T) = \begin{cases} \tau_1 & \text{if } T \le Ac1 \\ \tau_1 + \frac{T-Ac1}{Ac3-Ac1}(\tau_3 - \tau_1) & \text{if } Ac1 \le T \le Ac3 \\ \tau_3 & \text{if } T \ge Ac3 \end{cases} \tag{8}$$

The value of τ_1 and τ_3 determined by experiment of thermal expansion corresponded to the time for quasi static temperature of start (Ac1) and end (Ac3) of austenite transformation.

During rapid cooling, the austenite with a face centered cubic structure changes to martensite with a body centered tetragonal structure. This phase transformation is described by the Koistinen and Marburger model [12].

$$z_m = z_0[1 - \exp[-\beta\langle M_s - T\rangle]] \tag{9}$$

Where $\langle x\rangle = 0 \ \forall x < 0 \ et \ \langle x\rangle = x \ \forall x \ge 0$, z_m is the proportion of martensite formed, z_0 is the proportion initial of austenite, M_s is the martensitic start temperature, β is a material parameter and T is the temperature in degree Celsius.

The volume fraction functions are resolved by the Euler explicit methods:

$$\boldsymbol{Z_{n+1} = Z_n + \dot{Z}_n.\Delta t} \tag{10}$$

$$\boldsymbol{\Delta t = t_{n+1} - t_n} \tag{11}$$

Where Zn+1 is the new volume fraction at time increment n+1, Zn is the volume fraction at the time increment n and Δt is the time increment.

2.3. Mechanical model

The resolution of the mechanical equation is based on the equation of static equilibrium [9].

$$\boldsymbol{div(\sigma) - F = 0} \tag{12}$$

Where σ is stress tensor and F is volume force.

The relationship of deformation is described in the following case

$$\boldsymbol{\epsilon = \varepsilon^e + \varepsilon^{th} + \varepsilon^p} \tag{13}$$

where ε^e is the thermal strain, ε^{th} is the transformation induced volume strain and ε^p is the plastic strain. The separation between the transformation induced volume strain and the thermal strain by changing the coefficient of thermal expansion allows having more flexibilities to describe the behavior of the material [9]. The phase transformation plays an important role in modeling the residual stresses [15]. To count these changes in volume, the thermal deformation is replaced by a thermo-metallurgical strain [3] or transformation induced volumetric strain [26]:

$$\varepsilon^{thm} = (1 - Z).\left(\alpha_\gamma\left(T - T_{\gamma ref}\right) - \Delta\varepsilon_{\alpha\gamma}^{20°C}\right) + Z.\left(\alpha_\alpha\left(T - T_{\alpha ref}\right)\right) \tag{14}$$

Where z is the proportion of α phase (FP, B, M), ε_α^{th}, ε_γ^{th} are respectively the thermal expansion of the phase α and γ. $\Delta\varepsilon_{\alpha\gamma}^{20°C}$ is the different thermal strain between the two phases. The volume change of DP600 steel [20] from austenite to ferrite is assumed to be 1.4 % and from austenite to martensite 1 % which is in accordance to values reported in the research [5, 11, 23].

2.4. Numerical model's Parameter

The thermal simulation by using Gaussian distribution conical heat source model in solid phase leads to higher maximum temperature, more than 3000˚C, in the center of the fusion pool that is much more difference from reality. The effect of fluid flow and solidification of material have significant effects on the temperature distribution and on the shape of weld pool. Deng proposed an artificially increased thermal conductivity to be approximately twice of the value at room temperature when the temperature is higher than the melting point temperature [6]. The thermal effects due to solidification of the weld pool by the influence of latent heat for fusion is supposed to be less influent on the results of the simulation [10], and it is not counted in this work. The thermal property of dual phase steel DP600 are presented in Tab.2. The convection coefficient 73.5 $W/m^2.K$ and emissivity of 0.25 is constant base on the result of [16] are used in this analysis.

The mechanical data of DP600 are presented in Tab.4. The thermo metallurgical expansion used in the elastoplastic model with volume change is considered to be constant in each phase is shown in Tab.3 where

the thermal expansion interpolated by these values during heating and cooling are presented in Fig.15(a) which is similar to the curves of experimental results of thermal expansion of DP600 steel [22].

The volume fraction of martensite is approximately 20% for DP600 steel [19, 1]. The growth parameter τ from ferrite, pearlite, bainite or martensite to austenite has been set to 0.05s in order to obtain a good agreement to the results of the phase field predictions for welding of DP600 reported by [24, 19]. Several investigations has showed that for very fast heating rates and low carbon contents, which occur in almost every weld, the end of gamma (γ) transformation does not depend on chemical composition, the Ac_3 was close to 910˚C for all grades of steel [18].

Table 3. Thermal property

Density of DP600	
0	7600
1000	7300
1200	7210
3000	7200

Thermo metallurgical expansion	
γ-base (Austenite)	$2.13\ 10^{-5}$
α-base (FM, M)	$1.68\ 10^{-5}$
$\Delta\varepsilon_{\alpha\gamma}^{25°C}$	0.01375

Thermal property of DP600			
Specific heat		*Conductivity*	
Temps	Heat	Temps	Cond
0	520	0	34.6
200	550	25	34.8
400	600	200	35
600	750	254	35
740	1160	1100	21.4
800	690	1200	25.5
1100	520	1300	60
1200	610	1400	70
3000	620	3000	70

Table 4. Mechanical property of DP600

Mechanical data for model EP					
Temperature	Expansion	Poison ratio	Elastic	$Yield_{0\%}$	$Yield_{0.02\%}$
0	1.2E-05	0.280	2.1E+11	3.8E+08	4.8E+08
300	-	0.295	1.9E+11	3.8E+08	4.6E+08
400	1.6E-05	-	-	3.8E+08	4.4E+08
550	-	-	-	3.1E+08	3.6E+08
600	-	0.310	1.2E+11	1.6E+08	2.3E+08
800	1.6E-05	0.330	3.0E+11	2.0E+07	8.0E+07
1000	2.2E-05	-	-	3.0E+06	1.0E+07
1200	2.5E-05	0.330	3.0E+11	3.0E+06	1.0E+07
3000	2.5E-05	0.330	3.0E+11	3.0E+06	3.0E+06

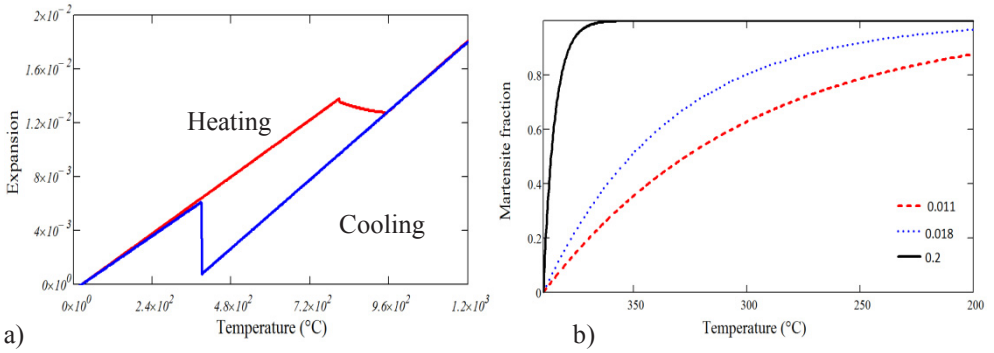

Fig. 1. Thermo-metallurgical expansion of DP600 (a), and Koistinen Marburger coefficient (b)

For higher rate of heating corresponded to laser welding, volume fraction of austenite is reach at the fusion temperature not Ac_3 [10], and Ac_1 is 720°C with temperature of fusion $T_{liquidus}$ equal to 1530°C [29] with the temperature of solidus $T_{Solidus}$ equal to 1440°C [22]. With higher value of material coefficient, β, of Koistiten-Marburger model, the transformation austenite to martensite complete around the martensite started temperature as showed in Fig.1 (b). A measurement data compared to numerical results at Gaussian point using a Koistinen-Marburger coefficient β, applied for DP600, equal to 0.011 or 0.018 as a standard value that does not fit in any case. A better approach can be found at a value of 0.2 with martensite start temperature Ms equal to 390˚C [17].

3. Simulation and preparation

The simulation is done in two states, the thermal state and mechanical state where three steps are considered, the welding step for 0.8823 seconds, the cooling step for 120 seconds and relaxing step for 120 seconds. The quadratic interpolation function gives more accurate results close to the weld seam and is used in this simulation to solve the thermal analysis of welding. The linear interpolation was used to solve the mechanical analysis.

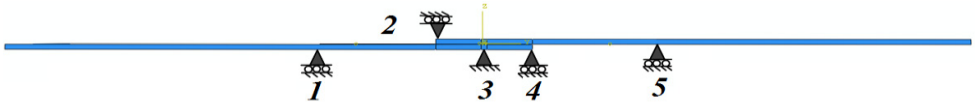

Fig. 2. Mechanical boundary condition

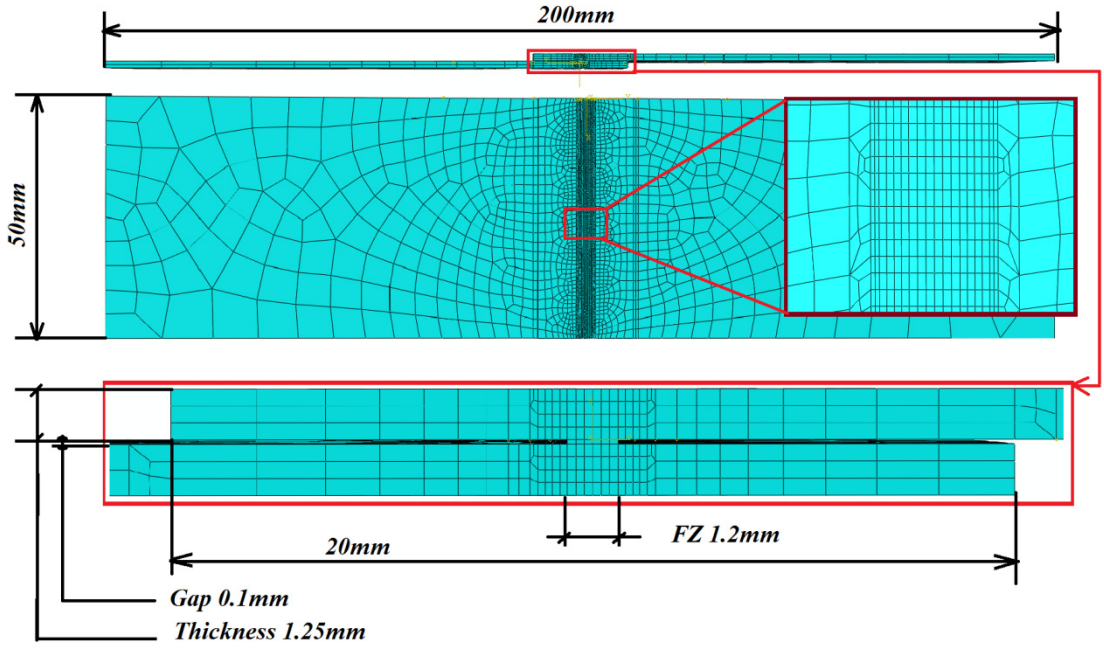

Fig. 3. Meshing element

Table 5. Mesh size of FZ and HAZ

	FZ-HAZ	Ratio in BM
DX	0.4mm	125:62:31:25:10
DY	0.2mm	biase 5:15
DZ	0.3125mm	4:3:2

The boundary condition plays an important role in the formation of residual stress and deformation of the welding joint. The nature of contact surface between the clamping system and the sheet metal is also influenced on the cooling rate of the welding process. Numerical predictions performed by Schwenk [4] for a case study where the cooling rate is increased by a factor of two.

The boundary conditions BCs, as illustrated in Fig.2, using in this model are:

- Position 1, 2, 4 and 5: Displacement Z =0 *(Z-SYMM mode)*. These BCs will relax at third step.
- Position 3: Lock the start of weld seam *(Encastre-mode)* and Displacement Z = 0 *(Z-SYMM-mode)* at the end of weld beam. These BCs are lock for all steps.

The model is separate into three zones, the FZ, the HAZ and the BM. The first order element with 8-nodes brick technique is used for the HAZ and the FZ in purpose to assure a constant and small element size inside these two zones. On the other hand the sweep technique with advancing front algorithm is used to reduce the number of elements inside the BM as shown in Fig.3. The mesh dimension of the FZ and the HAZ are presented in the Tab.5.

4. Results and discussion

4.1. Thermo metallurgical results

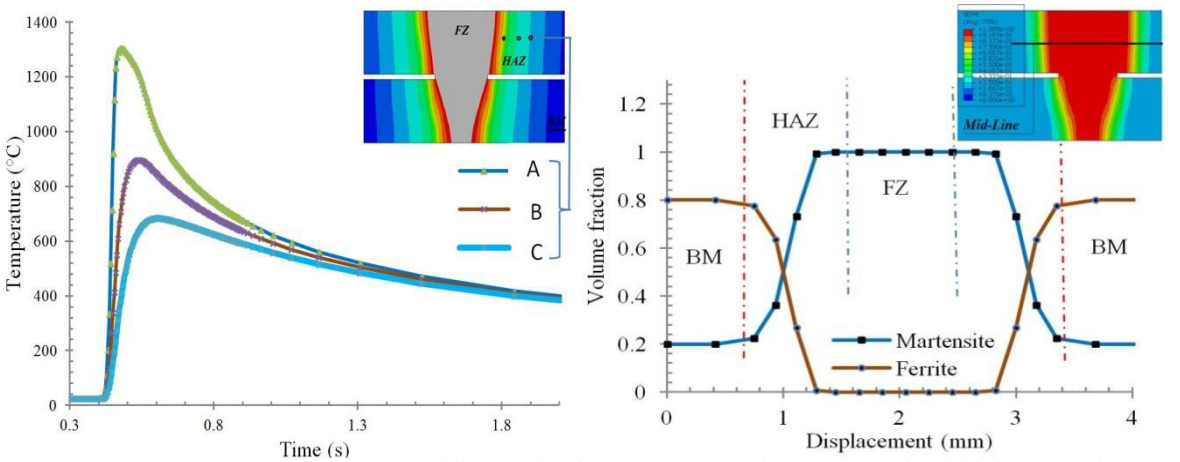

Fig. 4. Temperature evolution during welding a) and Volume fraction across the weld zone at the middle line of top sheet (b)

The thermal results of welding simulation are shown in Fig. 4 (a) in which the distribution of temperature at different points is presented. The temperature drops rapidly from the maximum temperature to around 500^0C in just one second as presented by the curve of points situated at points A, B and C *(at a distance of 0.95mm, 1.3mm and 1.6 mm from weld centre line respectively)*. The higher speed laser welding leads to faster cooling inside the FZ and HAZ that cause indifferent in metallurgical transformation at those points. These values are close to the cooling time in previous work [22].

Fig.4(b) showed the distribution of volume fraction along the mid-line of the top sheet. The formation of martensite and ferrite in the base metal (BM), the heat affected zone (HAZ) and the fusion zone (FZ) at the end of relaxation are evaluated. The higher volume fraction of martensite is the results of fast cooling rate inside the FZ and the HAZ as shown in Fig.4(a).

4.2. Thermo-mechano-metallurgical results

The effect of transformation induced volume strain on elastoplastic model is observed based on the residual stresses analysis such as longitudinal stresses S11 and transverse stresses S22 of the elastoplastic model, *EP model*, shown in Fig.5 (a, c) and those of elastoplastic model with transformation induced volume strain model, *VEP model*, presented in Fig.5(b, d).

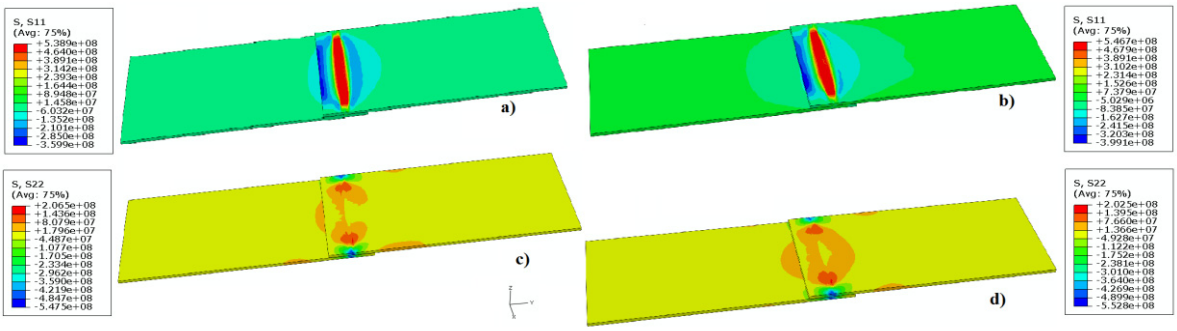

Fig. 5. Residual stresses from EP model (a,c) and VEP model (b,d)

The general aspects of residual stresses of these models are almost similar. But a few different aspects of residual stresses are found. The longitudinal residual stresses distribution along the transverse direction of VEP model, Fig.5 (b), is wider than that of the EP model, Fig.5 (a). The transverse residual stresses of VEP model, Fig6.5 (d), seem to give higher value than that of EP model, Fig.5 (c).

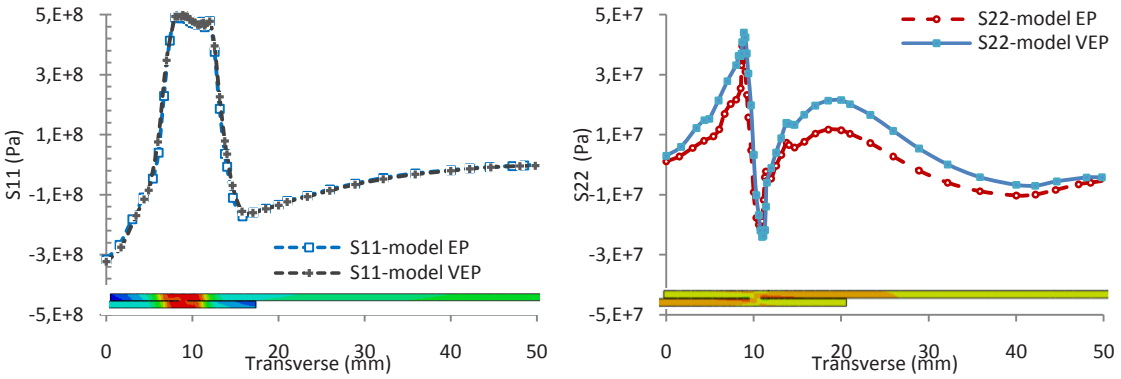

Fig. 6. Longitudinal residual stresses S11 and Transverse residual stresses S22 along the top-right transverse line

A further analysis are based on the study of residual stresses distribute along the transverse line in Fig.6. The comparison of residual stresses along the transverse line is the longitudinal residual stresses S11 and the transverse residual stresses S22. The curves proved that the residual stresses of these models followed the same distribution with just a few different *MPa* on its intensity was found. The VEP model gives a higher value of the longitudinal residual stresses S11, the transverse residual stresses S22 than those of the EP model. The difference can be considered to be negligible small. The longitudinal residual stresses of Nd:YAG laser welding applied to DP is in tensile state in the FZ of the weld joint. The same conclusion was found in [13].

5. Conclusion

The effect of transformation induced volumetric strain had been identified. The global distribution of residual stresses such as the longitudinal residual stresses and the transverse residual stresses show clearly the different residual stresses from these models. The VEP model gives a slightly higher value of longitudinal residual stresses S11 and transverse residual stresses S22 than that of the EP model. Anyway the different of

residual stresses of these models is very low and can be consider being negligible small. One can conclude that the transformation induced volume strain has less affect on the results of the elastoplastic model for the residual stresses analysis of laser welding.

Acknowledgements

This research work cannot work out without funding support from French Government Scholarship under a PhD Scholarship program. Not forgetting the technical and the material support from Maupertuis Institute for laser welding process, DP600 sheet metal supplied by Arcelor Mittal France.

References

[1] G. Avramovic-Cingara, Y. Ososkov, M.K. Jain, and D.S. Wilkinson. Effect of martensite distribution on damage behaviour in dp600 dual phase steels. *Materials Science and Engineering: A*, 516(1-2):7 – 16, 2009.

[2] Z. Zacharia B. Taljat, B. Radhakrishnan. Numerical analysis of gta welding process with emphasis on post-solidification phase transformation effects on residual stresses. *Mater. Sci. Eng*, A246:45–54, 1998.

[3] Jean-Michel BERGHEAU. Modélisation numérique de soudage. *Technique de l'ingénieur*, 2004.

[4] K. Dilger V. Michailov C. Schwenk, M. Rethmeier. Schweißsimulation im fahrzeugbau - möglichkeiten, grenzen und herausforderungen. Technical report, DVS Report, Nr. 237, pp. 353, 2005.

[5] M. Hidekazu D. Dean. Prediction of welding residual stress in multi-pass butt-welded modified 9cr–1mo steel pipe considering phase transformation effects. *Computational Material Science*, 37:209–216, 2006.

[6] Dean Deng. Fem prediction of welding residual stress and distortion in carbon steel considering phase transformation effects. *Materials & Design*, 30(2):359 – 366, 2009.

[7] Waeckel F. Modélisation du comportement thermo-métallurgique des aciers. volume 4. EDP Sciences, févier 1994.

[8] D. Gery, H. Long, and P. Maropoulos. Effects of welding speed, energy input and heat source distribution on temperature variations in butt joint welding. *Journal of Materials Processing Technology*, 167(2-3):393–401, 2005.

[9] John A. Goldak. *Computational Welding Mechanics*. Springer, 2005.

[10] Christophe Grignon, Eric Petitpas, Robert Perinet, and Jean Condoure. Modélisation thermométallurgique appliquée au soudage laser des aciersthermometallurgical modeling applied to laser welding of steels. *International Journal of Thermal Sciences*, 40(7):669 – 680, 2001.

[11] G.S. Ansell J.M. Moyer. The volume expansion accompanying the martensite transformation in iron-carbon alloys. *Metallurgical Transactions*, 6A:1785–1791, 1975.

[12] D.P. Koistinen and R.E. Marburger. A general equation prescribing the extent of the austenite-martensite transformation in pure iron-carbon alloys and plain carbon steels. *Acta Metallurgica*, 7(1):59 – 60, 1959.

[13] Fanrong Kong and Radovan Kovacevic. 3d finite element modeling of the thermally induced residual stress in the hybrid laser/arc welding of lap joint. *Journal of Materials Processing Technology*, In Press, Accepted Manuscript:–, 2010.

[14] J.B. Leblond and J. Devaux. A new kinetic model for anisothermal metallurgical transformations in steels including effect of austenite grain size. *Acta Metallurgica*, 32(1):137 – 146, 1984.

[15] Lars-Erik Lingren. *Computational Welding Mechanics: Thermomechanical and microstructural simulations*. Woodhead Publishing in Materials, 2007.

[16] P. Martinson, S. Daneshpour, M. Koçak, S. Riekehr, and P. Staron. Residual stress analysis of laser spot welding of steel sheets. *Materials & Design*, 30(9):3351 – 3359, 2009.

[17] M.Brand and D.Siegele. Numerical simulation of distortion and residual stresses of dual phase steels weldments. In *IIW-1820-07*, 2007.

[18] Ph.Bourges, L.Jubin, and P. Bocquet. Prediction of mechanical properties of weld metal based on some metallurgical assumptions. *Mathematical Modelling of Weld Phenomena*, pages 201–212.

[19] T. Schenk, I.M. Richardson, M. Kraska, and S. Ohnimus. Non-isothermal thermomechanical metallurgical model and its application to welding simulations. *Science and Technology of welding and joining*, 14(2):152–160, 2009.

[20] Tobias Schenk. *Modeling welding Distortion Influence of Clamping and Sequencing*. PhD thesis, Material Innovation Institute, www.m2i.nl, 2011.

[21] H. Schumann. *Metallographie*. ISBN: 3342004312, 1991.

[22] Christopher Schwenk. *FE-Simulation des Schweißverzugs laserstrahlgeschweißter dünner Bleche :Sensitivitätsanalyse durch Variation der Werkstoffkennwerte*. PhD thesis, Bundesanstalt für Materialforschung und prüfung, 2007.

[23] J. Sietsma M. T. RekveldtS. Van der Zwaag S.G.E. Velthuis, J.H. Root. The ferrite and austenite lattice parameters of fe-co and fe-cu binary alloys as a function of temperature. *Acta Materialia*, 46(15):5223–5228, 1998.

[24] R.G. Thiessen, I.M. Richardson, and J. Sietsma. Physically based modelling of phase transformations during welding of low-carbon steel. *Materials Science and Engineering: A*, 427(1-2):223 – 231, 2006.

[25] Muhammad Zain ul abdein. *Experimental investigation and numerical simulation of laser beam welding induced residual stresses and distortion in AA6056-T4 Sheets for Aeronautic application*. PhD thesis, 2009.

[26] Yannick Vincent, Jean-Michel Bergheau, and Jean-Baptiste Leblond. Viscoplastic behaviour of steels during phase transformations. *Comptes Rendus Mecanique*, 331(9):587 – 594, 2003.

[27] Anrieux S. Waeckel F. Thermo-metallurgical modelling of steel cooling behaviour during quenching or welding. In *14th Internatiinal Conference on Structural Mechanics in Reactor Technology (SMiRT), Lyon, France*, August 17-22, 1997.

[28] P. Dupas Waeckel F. and Andrieux. A thermo-metallurgical model for steel cooling behaviour: Proposition, validation and comparison with the sysweld's model. In *Journal de physique IV*, volume 6. EDP Sciences, Janvier 1996.

[29] Mingsheng XIA and Elliot BIRO. Effects of heat input and martensite on haz softening in laser welding of dual phase steels. *ISIJ International*, 48(6):809–814, 2008.